NANO LETTERS

Letter

pubs.acs.org/NanoLett

A Chemically-Responsive Nanojunction within a Silver Nanowire

Wendong Xing,[†] Jun Hu,[‡] Sheng-Chin Kung,[†] Keith C. Donavan,[†] Wenbo Yan,[†] Ruqian Wu,*[,‡] and Reginald M. Penner*[,†,§]

[†]Department of Chemistry, University of California, Irvine, California 92697-2025, United States,

[‡]Department of Physics, University of California, Irvine, California 92697-4575, United States, and

[§]Department of Chemical Engineering and Materials Science, University of California, Irvine, California 92697-2700, United States

Supporting Information

ABSTRACT: The formation of a nanometer-scale chemically responsive junction (CRJ) within a silver nanowire is described. A silver nanowire was first prepared on glass using the lithographically patterned nanowire electrodeposition method. A 1−5 nm gap was formed in this wire by electromigration. Finally, this gap was reconnected by applying a voltage ramp to the nanowire resulting in the formation of a resistive, ohmic CRJ. Exposure of this CRJ-containing nanowire to ammonia (NH_3) induced a rapid (<30 s) and reversible resistance change that was as large as $\Delta R/R_0$ = (+)138% in 7% NH_3 and observable down to 500 ppm NH_3. Exposure to water vapor produced a weaker resistance increase of $\Delta R/R_{0,H_2O}$ = (+)10−15% (for 2.3% water) while nitrogen dioxide (NO_2) exposure induced a stronger concentration-normalized resistance decrease of $\Delta R/R_{0,NO_2}$ = (−)10−15% (for 500 ppm NO_2). The proposed mechanism of the resistance response for a CRJ, supported by temperature-dependent measurements of the conductivity for CRJs and density functional theory calculations, is that semiconducting p-type Ag_xO is formed within the CRJ and the binding of molecules to this Ag_xO modulates its electrical resistance.

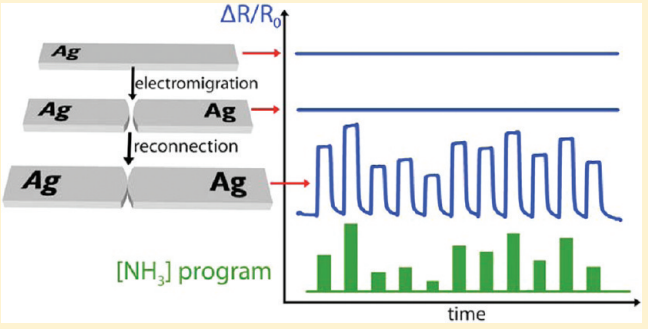

KEYWORDS: *Sensor, ammonia, nitrogen dioxide, electrodeposition, oxide, electromigration*

Nanowire field effect transistors have dominated work in the area of nanowire-based sensing since their discovery by Lieber et al. in 2001.[1] These devices, which are based upon semiconducting nanowires composed of In_2O_3,[2] Si,[1,3] or single walled carbon nanotubes (SWNTs),[4,5] operate based upon the same charge-gating principle exploited by ion-selective field-effect transistors (ISFETs) first described by Bergveld in the early 1970s.[6,7] Metal oxide nanowires, especially those of SnO_2,[8−10] have also been successfully implemented as gas sensors but charge gating in these materials can involve reactions of analyte molecules with reactive surface oxygen species.[11,12]

Metal nanowires cannot detect molecules by a charge gating mechanism because of their high carrier concentrations. However two other mechanisms for the detection of molecules have been demonstrated at metal nanowires. The first involves the inelastic surface scattering of electrons at wire surfaces, a process first described for ultrathin metal films by Fuchs in 1938.[13] The adsorption of molecules on the metal surface increases the cross-section for inelastic scattering and, provided the film or nanowire has dimensions that approach the mean free path for electrons (e.g., ∼40 nm for gold[14]), this results in an increased electrical resistance for the film or nanowire. The magnitude of this effect is relatively small for metal films with $\Delta R/R_0$ < 5%,[15,16] but Bohn et al. observed $\Delta R/R_0$ up to 10% for the adsorption of n-alkane thiols on gold nanowires.[17−19] N.J. Tao et al.[20−23] have reported a second mechanism that operates at metal nanowires with widths of 1 nm and below. Such nanowires show a conductivity that is quantized in units of $2e^2/h$. Exposure to adsorbates, including mercaptopropionic acid, 2,2′-bipyridine, and dopamine induces a transition to a lower conductivity state, corresponding to an increased resistance of up to 100%, for these junctions.[22]

In 2005, we discovered that the resistance of electrodeposited, polycrystalline silver nanowire arrays could increase dramatically, with $\Delta R/R_0$ up to 1000%, upon exposure to NH_3 vapor.[24,25] By interrogating these nanowires during NH_3 exposure using a conductive atomic force microscope tip, we discovered that the increased resistance induced by NH_3 exposure was concentrated at short, submicrometer sections of these nanowires, not uniformly distributed along the length of the nanowire.[25] On the basis of this and other data,[24,25] we hypothesized that at these "chemically responsive junctions" consisted of semiconducting Ag_xO layers that were embedded at grain boundaries present in the silver nanowire.[24,25]

Received: February 1, 2012
Revised: February 16, 2012
Published: February 23, 2012

Consistent with this proposed mechanism, we found that solid Ag_xO nanowires also exhibited a response to NH_3 that was indistinguishable to that seen at silver nanowires.[26] The formation of chemically responsive junction (CRJ) in our silver nanowire experiments, however, was uncontrolled with some nanowires containing several CRJ structures and others containing none. Consequently, the resistance sensitivity of arrays of these nanowires to NH_3 was characterized by enormous variability with some nanowire arrays showing no response to NH_3 at all and approximately 5% showing a large response exceeding $\Delta R/R_0$ = 100%.[24,25]

Here, we demonstrate that a single chemically responsive junction can be prepared within a single silver nanowire using a series of three processing steps (Figure 1). The first step is the

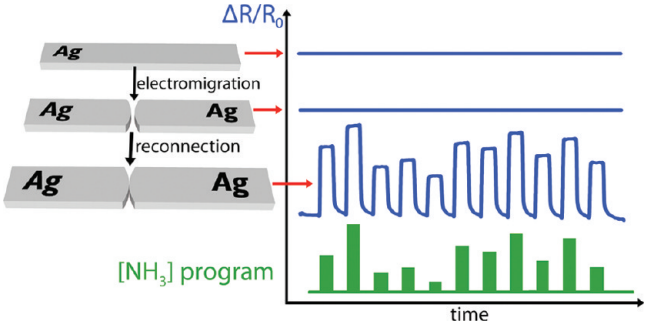

Figure 1. Schematic depiction of the formation of a CRJ within a silver nanowire. Starting with a silver nanowire (top), a nanogap is formed by feedback-controlled electromigration (middle). Neither the as-fabricated silver nanowire, nor the electromigrated nanowire, show a significant change in resistance upon exposure to pulses of NH_3. But when the nanogap is reconnected by the application of a voltage ramp (bottom), the resulting nanowire shows a rapid, reversible increase in its electrical resistance upon exposure to NH_3 as well as other molecules.

fabrication by lithographically patterned nanowire electrodeposition (LPNE)[27−29] of a single silver nanowire on a glass surface (Figure 1, top). In the second step, a nanogap with dimensions of 1−5 nm is introduced into this nanowire by feedback-controlled electromigration,[30] increasing the resistance of a 10 μm length of the nanowire from 100 to 300 Ω to 100 MΩ or higher (Figure 1, middle). Neither the as-prepared silver nanowire nor the electromigrated nanowire shows an appreciable change in resistance upon exposure to NH_3. Finally, a CRJ is created by reconnecting the nanogap, which is accomplished by applying a voltage ramp to 5 V (Figure 1, bottom). The reconnected nanowire now shows an ohmic electrical response with a resistance in the MΩ range that, as shown schematically in Figure 1, is reversibly modulated by exposure to NH_3. In this paper, we document the stepwise process for creating a CRJ-containing nanowire and we probe the properties of these unique and potentially useful structures for the detection of molecules.

The three-step process of CRJ formation (Figure 2) begins with the fabrication by LPNE of a silver nanowire and the preparation by evaporation of four-point electrical contacts (Figure 2a,b). This nanowire has typical lateral dimensions of 40 nm (h) and 150 nm (w) and is initially 100 μm or more in length, but the electrical contacts isolate a 10 μm length of the nanowire (Figure 2b). A nanogap is then formed between the inner electrical contacts using electromigration controlled by a LabVIEW algorithm as previously described.[30] Briefly, this

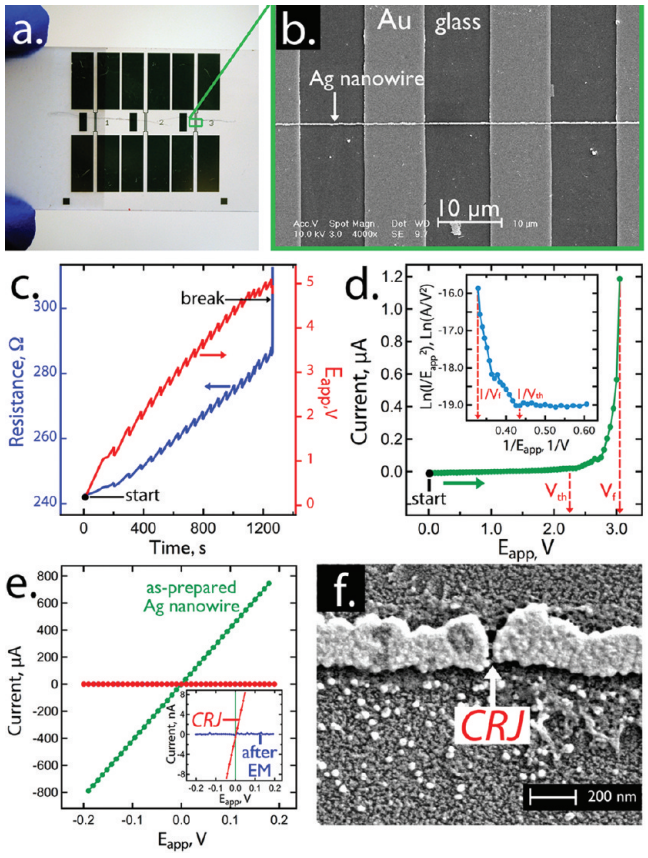

Figure 2. Formation of a CRJ. (a) Photograph of a 1 in × 2 in microscope glass slide with three sets of four-point probes used to electrically characterize the nanowire and to form the CRJ. (b) SEM showing four gold electrodes separated by 10 μm, and a silver nanowire spanning these four electrodes. (c) A nanogap is first formed within the silver nanowire using feedback-controlled electromigration, as previously described. Here, the nanowire resistance and the applied potential (E_{app}) are plotted as a function of time during the electromigration process. This nanogap is 1−5 nm in width. (d) Reconnection of the nanogap is accomplished by applying a linear voltage ramp. Shown here is a typical current versus voltage plot of the reconnection process. (Inset) Fowler-Nordheim plot of the reconnection process. (e) I−V curves of the as-fabricated, electromigrated, and reconnected nanowire. (Inset) Same data with rescaled current axis showing ohmic response of a CRJ. (f), High-magnification SEM image of a CRJ within a reconnected nanowire.

algorithm includes the following steps: (1) the application of an initial voltage bias ($E_{app,i}$ = 10−100 mV) and the measurement of an initial wire resistance, R_0; (2) the increase of E_{app} at a rate of 5 mV/s while the wire resistance is continuously measured; and (3) the stepwise reduction of E_{app} by 0.2 V whenever the resistance change ratio $(R - R_0)/R_0$ exceeds a predefined threshold (typically +1.5%). After this occurs, steps (2) and (3) are repeated until the program terminates when the formation of a nanogap is signaled by the measurement of R > 10 kΩ (at ∼1300 s in Figure 2c). The decrease in E_{app} at step (3) generates the sawtooth pattern seen in both the applied voltage (Figure 2c, red trace) and resistance (blue trace) measured during this process.[30] Once the nanogap is formed, R > 100 MΩ and the nanowire does not respond to NH_3. To reconnect the nanogap and form a CRJ, a voltage ramp is again applied across the nanowire (Figure 2d). In this case, E_{app} is increased from 0 V at 50 mV/s while the tunneling current is monitored.

dx.doi.org/10.1021/nl300427w | Nano Lett. 2012, 12, 1729−1735

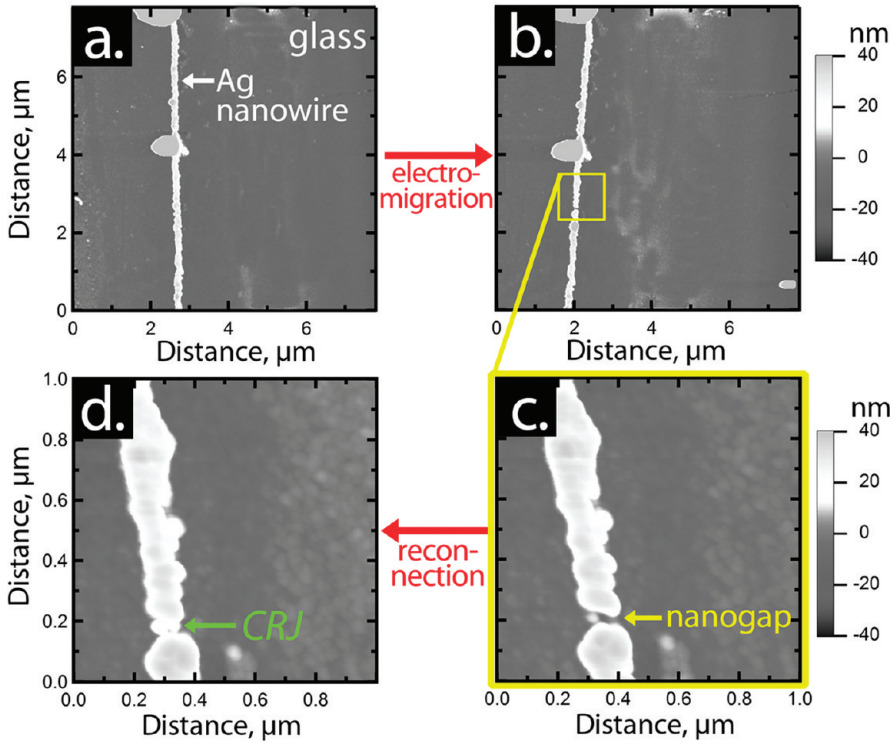

Figure 3. Tracking the formation of a CRJ using AFM. (a) An 8 μm section of a silver nanowire. Two defects, seen at top and center, provide reference points along the nanowire axis. (b) Same nanowire section after the formation within the yellow square of a nanogap by feedback-controlled electromigration. (c) Same nanogap shown at higher magnification. (d) Same area shown after reconnection and formation of a CRJ.

An increase in the current above baseline is seen at a threshold voltage, V_{th} = 2.25 V (Figure 2d), corresponding to a change in the slope of the Fowler–Nordheim (F-N) plot of $\mathrm{Ln}(I/V^2)$ versus $1/V$ (Figure 2d, inset). This deviation from an ideal linear slope in F-N plot is explained by a transition from thermionic to field emission as E_{app} increases.[31] The voltage bias was removed when the measured current exceeds 1 μA, at a final applied voltage (V_f) of 3.05 V in Figure 2d, signaling the reconnection is complete. A comparison of the current versus voltage curves obtained after each of the first three steps of this process (Figure 2e) shows the high electrical conductivity of the as-fabricated silver nanowire (R = 241 Ω, green trace), the disconnected nanowire after electromigration (R > 1 GΩ, Figure 2e, inset: blue trace) and the intermediate resistance of the CRJ after reconnection (R = 5.5 MΩ, red trace). A typical CRJ structure produced by this three-step procedure is seen in the high-magnification scanning electron micrograph (SEM) image of Figure 2f.

The formation of a CRJ can be monitored using atomic force microscopy (Figure 3). An 8 μm length of an as-fabricated Ag nanowire is seen in the atomic force microscopy (AFM) image of Figure 3a, together with two defects, one at the top and a second near the middle of the imaged region of the nanowire. After electromigration, the same section of nanowire was imaged again and the nanogap can be observed (Figure 3b). At higher magnification (Figure 3c), this nanogap has a minimum width of ~5 nm and a 4–5 nm island can be seen within the gap itself. After reconnection and formation of the CRJ, the nanogap closes and subtle changes in the morphology of the adjacent silver grains can be observed (Figure 3d). Our success rate for preparing CRJ that respond reversibly to ammonia is approximately 20%.

The resistance response of the silver nanowire to NH_3 is dramatically altered by the formation of a CRJ. An as-fabricated silver nanowire shows a slow decrease in its resistance ($\Delta R/R_0 \approx -1.3\%$) during exposures to pulses of NH_3 in N_2 ranging in concentration from 200 ppm to 7% (Figure 4a). The total change in R is virtually constant across this range of NH_3 concentrations, that spans a factor of 350. Ammonia is known from UHV studies to adsorb molecularly, without decomposition, on silver surfaces, to form hydrogen-bonded multilayers, and to desorb over a broad temperature range from 145 to 210 K.[32,33] The observed reversibility of the resistance change seen in Figure 4a, then, is presumably caused by the spontaneous desorption of NH_3 from the nanowire surfaces at ~300 K, and is consistent with the known behavior of NH_3 on silver surfaces in vacuum. After the formation of a CRJ, the baseline resistance of the nanowire, R_0, is elevated by a factor of 17 500 and exposure to NH_3 causes an abrupt increase in R with $\Delta R/R_0$ ranging from 1 to 2% at 200 ppm to 138% at 7% (Figure 4b). A similar resistance response is observed for exposures of the CRJ to methyl amine (CH_3NH_2) and dimethyl amine ($(CH_3)_2NH$) (Supporting Information, Figure S1). When plotted as $\Delta R/R_0$ (Figure 4c), the decreased resistance of an as-fabricated silver nanowire upon exposure to 2, 5, and 7% NH_3 is imperceptible as compared to the increased resistance of a CRJ. At all of the NH_3 concentrations, the R versus time transient has a peaked shape with R first increasing in 20–30 s to a maximum R value and then decaying during the NH_3 exposure. Similar behavior has been observed in prior work involving the detection of NH_3 at tungsten oxide nanowire mats[34] and vertical arrays of silicon nanowires[3] but the origin of this effect is not yet understood. When NH_3 is turned off, a rapid decrease of R in ~30 s is followed by a slow exponential decay with a time constant of 200–800 s (Figure

dx.doi.org/10.1021/nl300427w | Nano Lett. 2012, 12, 1729–1735

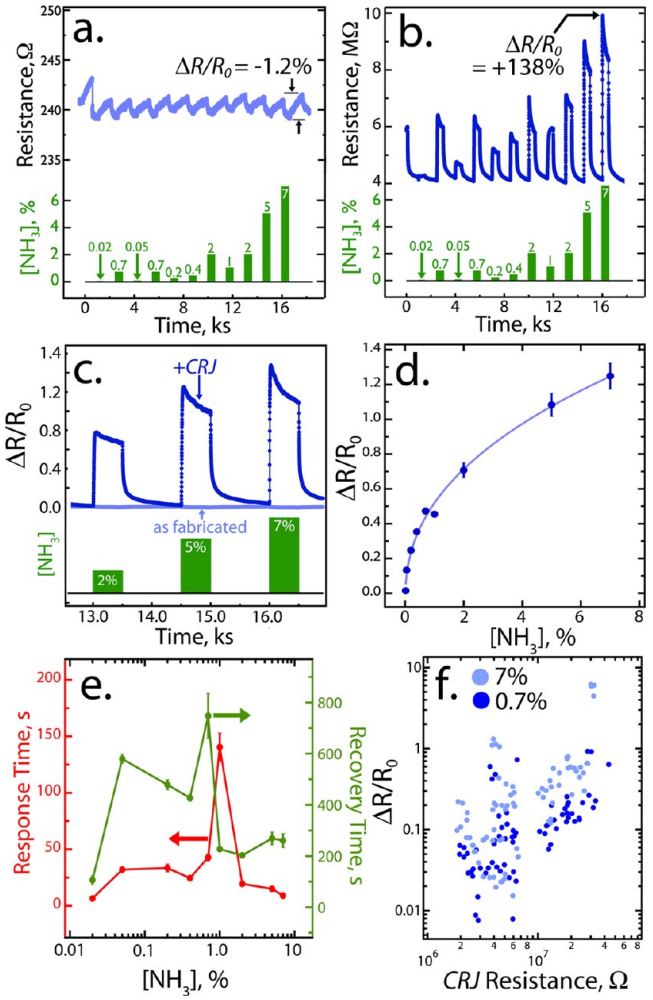

Figure 4. Response to NH_3 of a silver nanowire and the same silver nanowire containing an embedded CRJ. (a,b) Resistance as a function of time for an as-fabricated silver nanowire (a) and a silver nanowire containing a CRJ (b) for exposures to NH_3 in flowing nitrogen at the indicated concentrations. (c) Normalized resistance of the last three cycles as a function of time for the as-fabricated nanowire (light blue) and the CRJ. (d) $\Delta R/R_0$ versus $[NH_3]$ calibration curve for the response of a CRJ. Error bars show $\pm 1\sigma$ for three replicate exposures to ammonia at each concentration point. (e) Response time (red) and recovery time (green) time vs $[NH_3]$ for the CRJ. Error bars show $\pm 1\sigma$ for three replicate exposures to ammonia at each concentration point. (f) Sensitivity ($\Delta R/R_0$) as a function of the CRJ resistance showing the correlation between these two variables for two different NH_3 concentrations as indicted.

4c). Thus, R response of a CRJ to NH_3 is a factor of 3 more rapid than recovery of the R to the baseline value in the absence of NH_3 (Figure 4e). A calibration plot for $\Delta R/R_0$ versus $[NH_3]$ (Figure 4d) shows downward curvature that is consistent with the progressive occupation of NH_3 binding sites on the CRJ with increasing NH_3 concentration.

Finally, we find that the sensitivity of the CRJ to NH_3 and the resistance of this structure in the absence of NH_3 (i.e., R_0) are correlated. In Figure 4f, we plot the $\Delta R/R_0$ measured for exposures to 7 and 0.7% NH_3 versus R_0 for seventeen different CRJ devices. For most of these devices, between 1 and 5 data points were obtained as R_0 shifted over time. Despite the considerable scatter, a clear correlation between R_0 and $\Delta R/R_0$ in ammonia is seen in these data. This trend reproduces the behavior seen for silver nanowire arrays in our earlier study.[25] In summary, the influence of a CRJ on NH_3 detection by a silver nanowire is (1) to invert the direction of the R change, (2) to increase by a factor of >100 the magnitude of this R change, and (3) to dramatically accelerate the time rate of change of R at the onset of NH_3 exposure.

What is a CRJ and how does it function? In an attempt to probe the nanometer-scale structure of CRJs we have examined these structures using transmission electron microscopy (Supporting Information, Figure S2) but it has been impossible to resolve compounds other than silver within them. The electronic properties of a CRJ, however, clearly diverge from those of the "parent" silver nanowire. We measured the temperature-dependent resistance for a silver nanowire across the temperature range from 200 to 300 K (Figure 5a) and then

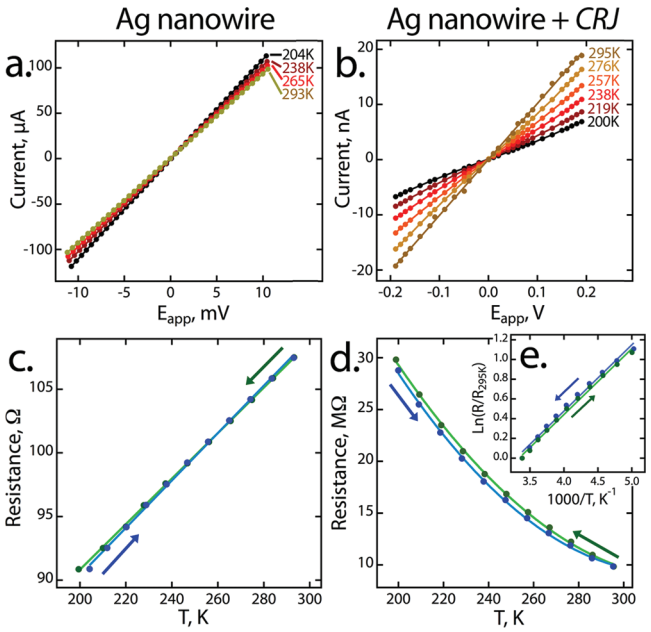

Figure 5. Temperature-dependent electrical properties of a silver nanowire and the same silver nanowire containing an embedded CRJ. (a,b) $I-V$ curves for an as-fabricated silver nanowire (a) and a CRJ-containing nanowire (b) over the temperature range from 200 to 295 K. (c,d) Resistance versus temperature for an as-fabricated silver nanowire (c) and a CRJ-containing nanowire (d) showing metallic (c) and semiconducting (d) behavior, respectively. (e) Arrhenius plot of the data shown in (d) from which an activation energy of 57.6 meV was derived.

fabricated a CRJ and repeated this measurement (Figure 5b). Current versus voltage curves are ohmic for both types of samples, but the metallic temperature dependence of the silver nanowire (Figure 5c) is replaced by a thermally activated conduction in the CRJ (Figure 5d). Specifically, for the silver nanowire R is directly proportional to the temperature

$$R = \alpha R_0 (T - T_0) \quad (1)$$

where R_0 and T_0 are the reference resistance and temperature, respectively, and α is the temperature coefficient of resistivity. For this nanowire, $\alpha = 1.96 \times 10^{-3}$ K^{-1}, which is somewhat smaller than the bulk value, 3.74×10^{-3} K^{-1}.[35] Qualitatively, this difference is expected based upon the greater prevalence in the nanowire of temperature-independent scattering mechanisms including surface and grain boundary scattering.[36] On the

dx.doi.org/10.1021/nl300427w | Nano Lett. 2012, 12, 1729–1735

other hand, the thermally activated behavior of the CRJ suggests that a semiconducting barrier to conduction now exists and its R versus T behavior is well described by an equation of the Arrhenius form

$$R = R_0 \exp\left(\frac{E_a}{kT}\right) \quad (2)$$

where E_a is the activation energy and k is Boltzmann's constant. An Arrhenius plot of these data is linear (Figure 5d, inset) and yields E_a = 57.6 meV. The observation of thermally activated transport through a CRJ suggests that conduction through this structure is controlled by a semiconducting domain and considering that CRJs are produced in air, a chemically reasonable candidate for the composition of this domain is Ag_xO. While precise measurements of the bandgap for nonstoichiometric Ag_xO are not available, Ag_2O is a semiconductor with a direct gap estimated at 1.3 eV[37] while AgO has an indirect gap of 1.2 eV.[38] Are the majority carriers within this Ag_xO electrons or holes? We answered this question by directly measuring the Seebeck coefficient, S, of Ag_xO film was generated by oxidation of silver metal, simulating the formation of a CRJ within a silver nanowire in air (Supporting Information, Figure S3).[39,40] Briefly, a 100 μm wide Ag_xO was formed by electrooxidation of an evaporated silver film located in a microfabricated chip which enabled the imposition of a temperature gradient, ΔT, along the nanowire while the Seebeck voltage, V_S, was simultaneously measured (Supporting Information, Figure S4).[39,40] The value of S is then given by[41]

$$S = \frac{-V_S}{\Delta T} = \frac{-(V_{hot} - V_{cold})}{T_{hot} - T_{cold}} \quad (3)$$

S values ranging from +13 to +25 μV/K were obtained over this temperature range (Supporting Information, Figure S4) indicating that holes are the majority carriers.

We used density functional theory (DFT) to test the hypothesis that a CRJ consists of an Ag_xO "gate". First, we studied the alternative possibility that the CRJ consists of an ultrathin Ag atomic chain or quantum point contact. On the basis of our DFT calculations of simulated all metal nanostructures, even a monatomic Ag chain is metallic (Figure S5 and Supporting Information). CRJs also fail to exhibit other attributes of sub-1 nm nanowires, such as quantized conductance.[20−23] Next, we constructed a nanoscopic Ag_xO conduit. We presumed a diameter of ∼1 nm for this structure, and we calculated a series of compositions, with x = 1.23, 1.37, 1.55, 1.78, and 2.0, using the ab initio molecular dynamics method. From the quadratic fitting for the formation energy versus x as in Supporting Information Figure S6, the equilibrium composition for this ultrathin Ag_xO wire is x = 1.56. This value should approach 2 when the diameter increases gradually. We chose the $Ag_{1.78}O$ nanowire as the prototype to investigate effects of NH_3 absorption on wires that are likely to be in the 1.0−2.0 nm range (Figure 6a,b).

We found that NH_3 molecules bind more strongly to Ag sites within this structure, forming strong Ag−N bonds and weaker O−H bonds, with binding energies ranging from 0.5 to 1.3 eV on different Ag sites (Table 1). The large adsorption energies (>1.0 eV) may account for the fast response and slow recovery of the resistance change observed. To study how the NH_3 adsorption electronically affects the transport property of the $Ag_{1.78}O$ nanowire, we choose one configuration with four NH_3 molecules on the $Ag_{1.78}O$ nanowire and give the charge transfer

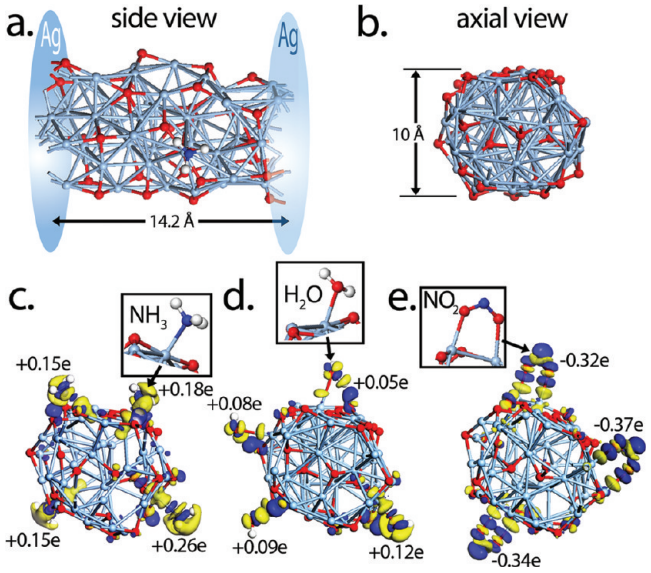

Figure 6. DFT model of a CRJ consisting of a Ag_xO conduit. (a,b) $Ag_{48}O_{27}$ (x = 1.78) conduit shown in side view (a) and axial view (b). Cyan and red spheres represent Ag and O atoms, respectively. (c−e) Axial views of the same bridge shown in (a,b) with chemisorbed NH_3 (c), H_2O (d), and NO_2 (e). Yellow and dark blue isosurfaces map charge differences [$\Delta\rho$ = ρ(bridge + molecules)ρ(bridge) − ρ(molecules)] with a cutoff of 0.02 e/Å^3. Yellow volumes denote charge depletion whereas dark blue volumes show charge accumulation. Numerical labels indicate the net charge state of each adsorbed molecule.

Table 1. Summary of DFT Results and Experimentally Observed Sensitivity for Exposures of a Single CRJ to NH_3, NO_2 and H_2O

gas	binding energy (eV)	charge transfer[a] (e)	exptl sensitivity[b] (%$^{-1}$)
NH_3	0.82 ± 0.59	+0.19 ± 0.09	0.22 ± 0.02
H_2O	0.60 ± 0.79	+0.09 ± 0.05	0.041 ± 0.004
NO_2, config A[c]	1.01 ± 0.08	−0.34 ± 0.04	−2.8 ± 0.1
NO_2, config B[c]	1.16 ± 0.18	−0.19 ± 0.08	

[a]Mean number of electrons transferred from each adsorbate molecule to the Ag_xO bridge. [b]Sensitivity in units of %$^{-1}$ was calculated for each gas as the relative resistance change normalized by the concentration of the gas exposure: $(\Delta R/R_0)$/[gas]%. Error bars represent $\pm 1\sigma$ for multiple gas exposures. [c]Configuration A refers to the bonding of NO_2 through the nitrogen to silver atoms in the Ag_xO bridge; configuration B refers to bonding through both oxygens to two silver atoms in the Ag_xO bridge.

plot in Figure 6c. Interestingly, all four NH_3 molecules donate electron charges to the $Ag_{1.78}O$ nanowire, and carry positive charges. The highest charge state is +0.26e, which means that 0.26 electron charge transfers from the NH_3 molecule to the $Ag_{1.78}O$ nanowire. The electrons transferred from NH_3 molecules compensate holes in the p-type $Ag_{1.78}O$ nanowire, leading to the increase in R observed experimentally. Therefore these DFT results provide an explanation of the resistance change upon NH_3 gas exposure and at a qualitative level the response and recovery times as well. A similar mechanism was also observed in copper oxide nanowires in our previous work.[42,43] Intriguingly, charge states on different sites scale with their binding energies: the greater the charge transfer, the

dx.doi.org/10.1021/nl300427w | Nano Lett. 2012, 12, 1729−1735

stronger the binding. Therefore, charge transfer actually plays two roles: binding and sensing.

To further validate this mechanism, we also investigated the effects on CRJ of two other analyte molecules: H_2O vapor and NO_2 gas both experimentally (Figure 7) and by DFT analysis

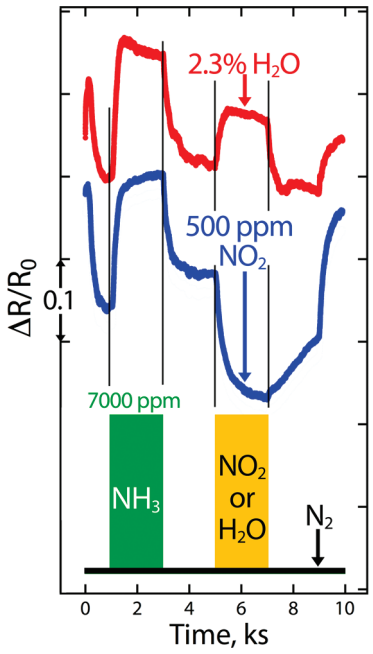

Figure 7. Response of a CRJ to H_2O and NO_2. Exposure to NH_3 increases the resistance, R, of a CRJ by $+0.22 \pm 0.02\%^{-1}$. Exposure to water vapor (red trace) produces a weaker increase in R ($+ 0.041 \pm 0.004\%^{-1}$) while exposure to NO_2 (blue trace) induces an even stronger decrease in R ($-2.8 \pm 0.1\%^{-1}$).

of the $Ag_{1.78}O$ nanowire (Figure 6d,e). Experimentally we find that H_2O induces an increase in R, but the sensitivity of a CRJ to water is just 20% as high as for NH_3 (Figure 7, red trace) while NO_2 induces a decrease in R with a sensitivity approximately an order of magnitude higher than seen for NH_3 (Figure 7, blue trace). In the context of the DFT calculations, we find that H_2O molecules form Ag−O bonds and that they also donate electrons to the $Ag_{1.78}O$ nanowire (Figure 6d, Table 1). One may predict that H_2O vapor causes a positive ΔR, just as observed experimentally (Figure 7). For NO_2 molecules, two different bonding configurations must be distinguished: (A) the N atom binds with Ag (Supporting Information, Figure S7), or (B) two O atoms bind with two Ag atoms (Figure 6e). The average binding energy of configuration A (~1.0 eV) is only slightly smaller than that of configuration B (1.1−1.3 eV). In both cases, NO_2 molecules take electron charges from the $Ag_{1.78}O$ nanowire (Figure 6e). The charge of configuration B is larger than that of configuration A, also in accordance with their binding energies (Table 1). Using the mechanism proposed above, the adsorption of NO_2 molecules should result in opposite resistance change in contrast to the case of NH_3 adsorption. Furthermore, the magnitude of charge transfer of NO_2 is higher than that of NH_3, so the nanowire should be more sensitive to NO_2 than to NH_3, just as seen in the experimental observations of Figure 7. On the basis of this analysis, we believe that the underlying physics or chemistry of the gas-induced resistance change through Ag nanowires is the charge transfer between adsorbates and Ag_xO at the CRJ region.

In summary, we have described a three step process for transforming a chemically unresponsive silver nanowire into a chemical sensor. More precisely, our process embeds a chemically responsive nanometer-scale junction within this silver nanowire. This three step process involves (1) nanowire growth, (2) nanogap formation by electromigration, and (3) reconnection of the nanogap and formation of the CRJ. The resistance of the CRJ responds rapidly and reversibly to the presence of amines, water vapor, and NO_2. A comparison of our experimental data with DFT calculations leads to the hypothesis that the CRJ consists of a p-type Ag_xO bridge approximately 1−2 nm in size, which is undetected in our TEM images of these structures. Further work will be required to optimize the sensitivity of the CRJ, to extend the limit-of-detection, and to enhance the selectivity of these structures for the detection of particular molecules. The CRJ represents a new enabling concept that should lead to the development of highly miniaturized sensors and sensor arrays based upon this new modality.

■ ASSOCIATED CONTENT

Ⓢ Supporting Information

Experimental procedures and materials required for the formation of nanojunctions and for the incorporation of these nanostructures into working sensors is provided as well as additional characterization data in the form of comparisons of the response of nanojunctions for three analyte molecules, transmission electron micrographs of nanojunctions, measurements of the thermopower for electrodeposited silver oxide films, and details relating to the DFT calculations. This material is available free of charge via the Internet at http://pubs.acs.org.

■ AUTHOR INFORMATION

Corresponding Author

*E-mail: (R.W.) wur@uci.edu; (R.M.P.) rmpenner@uci.edu.

Notes

The authors declare no competing financial interest.

■ ACKNOWLEDGMENTS

R.M.P. gratefully acknowledges the financial support by the National Science Foundation (CHE-0956524) and the School of Physical Sciences, Center for Solar Energy at UCI. R.W. acknowledges support from DOE, Grant DE-FG02-05ER46237, and computing time on supercomputers at NERSC. Electron microscopy was performed at the Materials Characterization Center, LEXI/CALIT2, at the University of California-Irvine.

■ REFERENCES

(1) Cui, Y.; Wei, Q.; Park, H.; Lieber, C. M. *Science* **2001**, *293*, 1289−1292.
(2) Li, C.; Zhang, D.; Lei, B.; Han, S.; Liu, X.; Zhou, C. *J. Phys. Chem. B* **2003**, *107*, 12451−12455.
(3) Field, C. R; In, H. J.; Begue, N. J.; Pehrsson, P. E. *Anal. Chem.* **2011**, *83*, 4724−4728.
(4) Collins, P. G.; Bradley, K.; Ishigami, M.; Zettl, A. *Science* **2000**, *287*, 1801−1804.
(5) Kong, J.; Franklin, N. R.; Zhou, C.; Chapline, M. G.; Peng, S.; Cho, K.; Dai, H. *Science* **2000**, *287*, 622−625.
(6) Bergveld, P. *IEEE Trans. Biomed. Eng.* **1970**, *BM17*, 70−76.
(7) Bergveld, P. *IEEE Trans. Biomed. Eng.* **1972**, *BM19*, 342−351.

(8) Kolmakov, A.; Klenov, D.; Lilach, Y.; Stemmer, S.; Moskovits, M. *Nano Lett.* **2005**, *5*, 667−673.
(9) Sysoev, V. V.; Goschnick, J.; Schneider, T.; Strelcov, E.; Kolmakov, A. *Nano Lett.* **2007**, *7*, 3182−3188.
(10) Thong, L. V.; Hoa, N. D.; Le, D. T. T.; Viet, D. T.; Tam, P. D.; Le, A.-T.; Hieu, N. V. *Sens. Actuators, B* **2010**, *146*, 361−367.
(11) Hieu, N. V.; Quang, V. V.; Hoa, N. D.; Kim, D. *Curr. Appl Phys.* **2011**, *11*, 657−661.
(12) Wei, A.; Xiaojun, W.; Zeng, X. *J. Phys. Chem. C* 5747−55.
(13) Fuchs, K. *Proc. Cambridge Philos. Soc.* **1938**, *34*, 100−108.
(14) Ashcroft, N. W.; Mermin, N. D. *Solid state physics*; Holt, Rinehart and Winston: New York, 1976.
(15) Hsu, C.-L.; McCullen, E. F.; Tobin, R. G. *Chem. Phys. Lett.* **2000**, *316*, 336−342.
(16) Tobin, R. G. *Surf. Sci.* **2002**, *502*−*503*, 374−387.
(17) Zhang, Y.; Terrill, R. H.; Bohn, P. W. *Anal. Chem.* **1999**, *71*, 119−125.
(18) Shi, P.; Zhang, J.; Lin, H.-Y.; Bohn, P. W. *Small* **2010**, *6*, 2598−2603.
(19) Zhang, Y.; Terrill, R. H.; Bohn, P. W. *J. Am. Chem. Soc.* **1998**, *120*, 9969−9970.
(20) Li, C. Z.; Sha, H.; Tao, N. J. *Phys. Rev. B* **1998**, *58*, 6775−6778.
(21) Li, C. Z.; He, H. X.; Bogozi, A.; Bunch, J. S.; Tao, N. J. *Appl. Phys. Lett.* **2000**, *76*, 1333−1335.
(22) Bogozi, A.; Lam, O.; He; Li; Tao, N. J.; Nagahara, L. A.; Amlani, I.; Tsui, R. *J. Am. Chem. Soc.* **2001**, *123*, 4585−4590.
(23) He, H.; Shu, C.; Li, C.; Tao, N. *J. Electroanal. Chem.* **2002**, *522*, 26−32.
(24) Murray, B. J.; Walter, E. C.; Penner, R. M. *Nano Lett* **2004**, *4*, 665−670.
(25) Murray, B. J.; Newberg, J. T.; Walter, E. C.; Li, Q.; Hemminger, J. C.; Penner, R. M. *Anal. Chem.* **2005**, *77*, 5205−5214.
(26) Murray, B.; Li, Q.; Newberg, J.; Hemminger, J.; Penner, R. *Chem. Mater.* **2005**, *17*, 6611−6618.
(27) Menke, E. J.; Thompson, M. A.; Xiang, C.; Yang, L. C.; Penner, R. M. *Nat. Mater.* **2006**, *5*, 914−919.
(28) Xiang, C.; Kung, S.-C.; Taggart, D. K.; Yang, F.; Thompson, M. A.; Gueell, A. G.; Yang, Y.; Penner, R. M. *ACS Nano* **2008**, *2*, 1939−1949.
(29) Kung, S. C.; Xing, W.; Donavan, K. C.; Yang, F.; Penner, R. M. *Electrochim. Acta* **2010**, *55*, 8074−8080.
(30) Xiang, C.; Kim, J. Y.; Penner, R. M. *Nano Lett.* **2009**, *9*, 2133−2138.
(31) Xu, N. S.; Chen, J.; Deng, S. Z. *Appl. Phys. Lett.* **2000**, *76*, 2463−2465.
(32) Gland, J. L.; Sexton, B. A.; Mitchell, G. E. *Surf. Sci.* **1982**, *115*, 623−632.
(33) Kwon, H.; Hwang, K.; Park, J.; Ryu, S.; Kim, S. K. *Phys. Chem. Chem. Phys.* **2011**, *13*, 17785−17790.
(34) Zhao, Y.; Zhu, Y. *Sens. Actuators, B* **2009**, *137*, 27−31.
(35) Calvert, J. *Copper, Silver, Gold*; 2002.
(36) Steinhogl, W.; Schindler, G.; Steinlesberger, G.; Traving, M.; Engelhardt, M. *J. Appl. Phys.* **2005**, *97*, 023706.
(37) Tjeng, L.; Meinders, M.; Vanelp, J.; Ghijsen, J.; Sawatzhy, G.; Johnson, R. *Phys. Rev. B* **1990**, *41*, 3190−3199.
(38) Allen, J. P.; Scanlon, D. O.; Watson, G. W. *Phys. Rev. B* **2010**, *81*, 161103.
(39) Taggart, D. K.; Yang, Y.; Kung, S.-C.; McIntire, T. M.; Penner, R. M. *Nano Lett.* **2011**, *11*, 125−131.
(40) Yang, Y.; Taggart, D. K.; Cheng, M. H.; Hemminger, J. C.; Penner, R. M. *J. Phys. Chem. Lett.* **2010**, *1*, 3004−3011.
(41) Ibach, H.; Lüth, H. *Solid-state Physics: An Introduction to Principles of Materials Science*, 4th ed.; Springer: Berlin, 2009.
(42) Hu, J.; Li, D.; Lu, J. G.; Wu, R. *J. Phys. Chem. C* **2010**, *114*, 17120−17126.
(43) Li, D.; Hu, J.; Wu, R.; Lu, J. G. *Nanotechnology* **2010**, *21*, 485502.